MERLIN: A flood hazard forecasting system for coastal river reaches

Ignacio Fraga[a], Luis Cea[b], Jerónimo Puertas[c]

[a] *ignacio.fraga@udc.es. ORCID: 0000-0001-5626-7781. CITIC. University of A Coruña, Spain. Corresponding author*

[b] *luis.cea@udc.es. ORCID: 0000-0002-3920-0478. Environmental and Water Engineering Group, Department of Civil Engineering, University of A Coruña, Spain,*

[c] *jeronimo.puertas@udc.es, ORCID: 0000-0001-6502-0799. Environmental and Water Engineering Group, Department of Civil Engineering, University of A Coruña, Spain,*

Abstract: This study presents MERLIN, an innovative flood hazard forecasting system for predicting discharges and water levels at flood prone areas of coastal catchments. Discharge forecasts are preceded by a hindcast stage. During this stage, the hydrological models assimilate soil moisture and hydro-meteorological observations to evaluate soil infiltration capacities at the beginning of the discharge forecast. Predicted discharges are converted to water level forecasts using the hydraulic model Iber+, a GPU parallelized bidimensional flow model. Hydraulic models also assimilate tidal level forecasts in order to define the boundary conditions of the models. The performance of MERLIN was evaluated over 4 months at 3 coastal catchments of 4.95, 16.96, and 83.9 km^2. Forecasted discharges and water levels presented a good fit to observed values, especially at the larger catchments, which confirmed the potential utility of the presented system.

Keywords: Flood hazard forecast; early warning system; hydraulic modelling; hydrological modelling; flood risk management.

This version of the article has been accepted for publication, after peer review (when applicable) and is subject to Springer Nature's AM terms of use, but is not the Version of Record and does not reflect post-acceptance improvements, or any corrections. The Version of Record is available online at: https://doi.org/10.1007/s11069-020-03855-7

1. Introduction

Flood events are becoming more frequent due to multiple factors. On the one hand, changes in land use and rapid urbanization have increased the amount of rainfall conveyed to streams (Rosburg et al., 2017). On the other hand, climate change has increased maximum rainfall intensities that increase river flood hazards at all the scales (Arnell and Gosling, 2016). In addition, the increase in the population has raised antropic pressure on water courses, and triggered the negative impact of flood events. As a result of all these factors, floods have become the main type of natural disaster, and in recent decades have affected 2.480 million people, causing damage worth 625 billion dollars according to the International Disaster Database (Wallemarq et al. 2018).

Against this background, several international organizations have proposed increasing resilience as a more efficient approach than building structural defences to reduce flood damage (Djordjevicet al. 2011; Schelfautet al., 2011). This approach has resulted in numerous flood forecasting systems, also known as early warning systems (EWS), at local (Cools et al. 2012, Hossain et al. 2014, Krajewski et al. 2017), national (Kellens et al. 2013, Weerts et al. 2011), and trans-national (Thielen et al. 2009) scales.

Currently, most flood forecasting systems are similar in structure. The operation of the system begins with the acquisition of meteorological data. This data usually consists of forecasts obtained from numerical weather prediction (NWP) models, which can achieve spatial resolutions of a few kilometres and temporal resolutions of less than an hour. The main drawback is that the accuracy of the forecasts depends largely on the time span of the predictions and on the rainfall aggregation time. The hydrological response of small catchments depends mostly on maximum rainfall intensities at low aggregation times. However, the accuracy of weather prediction models diminishes as does the rainfall aggregation time. In addition, flood forecasts require accurate

predictions of storm motion, since small deviations of the path of a storm can significantly affect the amount of rainfall in a catchment (particularly in small basins). These factors limit the applicability of NWP products for time horizons beyond a few days. An approach overcoming this limitation involves the use of meteorological and hydrological observations of gauges located upstream from the area under study. Though this approach has been employed in medium sized catchments (Ehret et al. 2008; Horita et al. 2018), it is more frequent in large basins (Nester et al. 2016; Krajewski et al. 2017), where flood propagation times are long enough to alert the population.

The second step of an EWS is to transform meteorological forecasts into discharge predictions. To this end, the most frequent approach is using physically based rainfall-runoff models. Satisfactory results have been reported using lumped (Alvarez-Garreton et al. 2015), semi-distributed (Oleyiblo and Li, 2010; Mure-Ravaud et al. 2016), and distributed (Thielen et al., 2009; Thiemig et al. 2015) models. Artificial intelligence techniques, such as neural networks (Kasiviswanathan et al. 2016), or genetic programming (Kumar and Sahay, 2018) have also been used for this purpose. These techniques reduce the computational burden of the forecast system, but fail to reproduce the physical processes involved; thus, accuracy and applicability are substantially constrained by the calibration data.

No matter what type of model is used to compute the rainfall-runoff transformation, reliable discharge forecasts require both accurate meteorological forecasts and a proper characterization of the antecedent soil moisture content (AMC). The same runoff can originate from high rainfall intensities falling over a relatively dry terrain or from low rainfall intensities falling over a saturated terrain. The improvement in the performance of rainfall-runoff computations when AMC is incorporated has been widely reported by

numerous authors (Brocca et al. 2011;Van Steenbergen and Willems, 2013; Massari et al. 2014; Tayfur et al. 2014; Massari et al. 2015; Cea and Fraga, 2018). An increase of nearly 50% in the correlation of the forecasted and observed discharges has been observed when the hydrological model was fed with AMC data (Lievens et al., 2015). Similarly, an increase of one order of magnitude in the accuracy of peak discharges was obtained when soil moisture data was used in an operational flood forecasting system (Wanders et al., 2017).

Most EWS assess flood hazard directly from the discharges computed by hydrological models. When discharges exceed a specific threshold, they are reported to stakeholders and the population through different channels (web apps, mail, acoustic alerts, etc.). An interesting review of the challenges during this last step of the flood forecasting process can be found in Schwanenberg et al. (2018).

Several EWS include a third step, in which the forecasted discharges are used as input of a hydraulic model to compute the spatial distribution of water depth and velocity. Hydraulic models allow for an accurate estimation of the flood extent, but their computational burden limits their application, so the number of flood forecasting systems including these types of model is scarce (Nguyen et al. 2016, Sanz Ramos et al. 2018). However, this last step is particularly crucial in coastal areas, where flooding is due to the combined effect of the tidal level and the river discharge (Acreman, 1994; Hawkes, 2003; Sopelana et al. 2018, Svensson and Jones, 2002). In these cases, the use of hydraulic models is essential to impose boundary conditions reproducing both the river discharge and sea level, allowing for an accurate estimation of the flood hazard that is not possible from only the output of a hydrological model. Moreover, including tidal levels in flood forecasting is becoming increasingly vital due to increasing sea levels resulting from climate change (IPCC, 2018).

In recent years, forecasting systems have improved considerably for two main reasons. First, remote observations such as meteorological radar and satellite observations are usually available in near real-time, and often at no cost. These observations, with high spatial (and sometimes temporal) resolution, allow for accurate hydro-meteorological monitoring that improves the quality and quantity of available data. The use of standard file formats and data transfer protocols facilitates the easy integration of these data sources to existing forecasting systems. Furthermore, the computational time needed to run high-resolution 2D flooding models has decreased significantly, thanks to High Performance Computing techniques and the increase of computational power (García-Feal et al. 2018; Nguyen et al. 2016; Noh et al. 2018; Sanders et al. 2019; Xia et al. 2019).

In this article we present MERLIN, a flood forecasting system that exploits these improvements to deliver discharge and flood extent forecasts on a daily basis from meteorological predictions. MERLIN (which is the acronym in Spanish for Local Flood Risk Evaluation Model) incorporates remote observations to characterize the initial soil infiltration capacity prior to the discharge forecast. Discharges are forecasted using numerical weather predictions that feed semi-distributed models of flood prone catchments. To forecast the flood extension, MERLIN uses the 2D inundation model Iber+ (García-Feal et al. 2018), which is a GPU-parallelized version of the Iber model (Bladé et al., 2014).

The MERLIN system has been used to forecast the flood hazard at several catchments in the region of Galicia (northwest Spain). The Special Civil Protection Plan for Flood Risks in Galicia (Xunta de Galicia, 2016), and the Flood Risk Management Plan of Galicia-Costa 2015–2021 (Augas de Galicia 2016), both acknowledge the need for developing hydrological forecast systems in this region to enhance decision making.

However, flood forecasting in Galicia is particularly challenging for two reasons. First, there are numerous small catchments in which discharge forecasting is highly sensitive to the spatial and temporal evolution of weather fronts. Secondly, most flood risk areas in Galicia correspond to coastal towns, where floods are caused by the joint effect of tidal level and river discharge. The MERLIN system was implemented at 3 coastal catchments with contributing areas of ≈5, 15, and 80 km^2 in order to explore the feasibility of the system in small basins, and to assess the effect of the catchment area on the performance of the forecasting system.

The paper is structured as follows. Section 2 provides a detailed description of the MERLIN system. Section 3 describes the characteristics of the catchments used to evaluate system performance. Section 4 reviews the application of the system during the winter of 2018 and the spring of 2019. Section 5 highlights the main conclusions of this study.

2. Description of the flood forecasting system

2.1. System overview and workflow

MERLIN forecasts the flood hydrographs and the flood hazard at the flood prone areas of selected catchments from meteorological observations and forecasts. MERLIN can be run on a daily or sub-daily basis. The functioning of the system consists of two stages: a hindcast stage and a forecast stage (Figure 1). During the hindcast stage, meteorological and discharge observations of the previous 30 days are assimilated by the hydrological models of the studied catchments in order to reproduce the soil moisture condition at the beginning of the forecast. A 30-day time window was selected due to the relation between soil moisture and the antecedent rainfall reported for areas in the northwest of Spain (Cea and Fraga, 2018). The relevance of this step should be

underscored owing to the impact of the previous moisture content on rainfall-runoff computations.

In the forecast stage, the hydrographs along the river network over the following days are predicted using meteorological forecasts and the initialized hydrological models. The predicted hydrographs are used as inputs of 2D hydraulic models of flood prone areas, in order to compute the flood hazard.

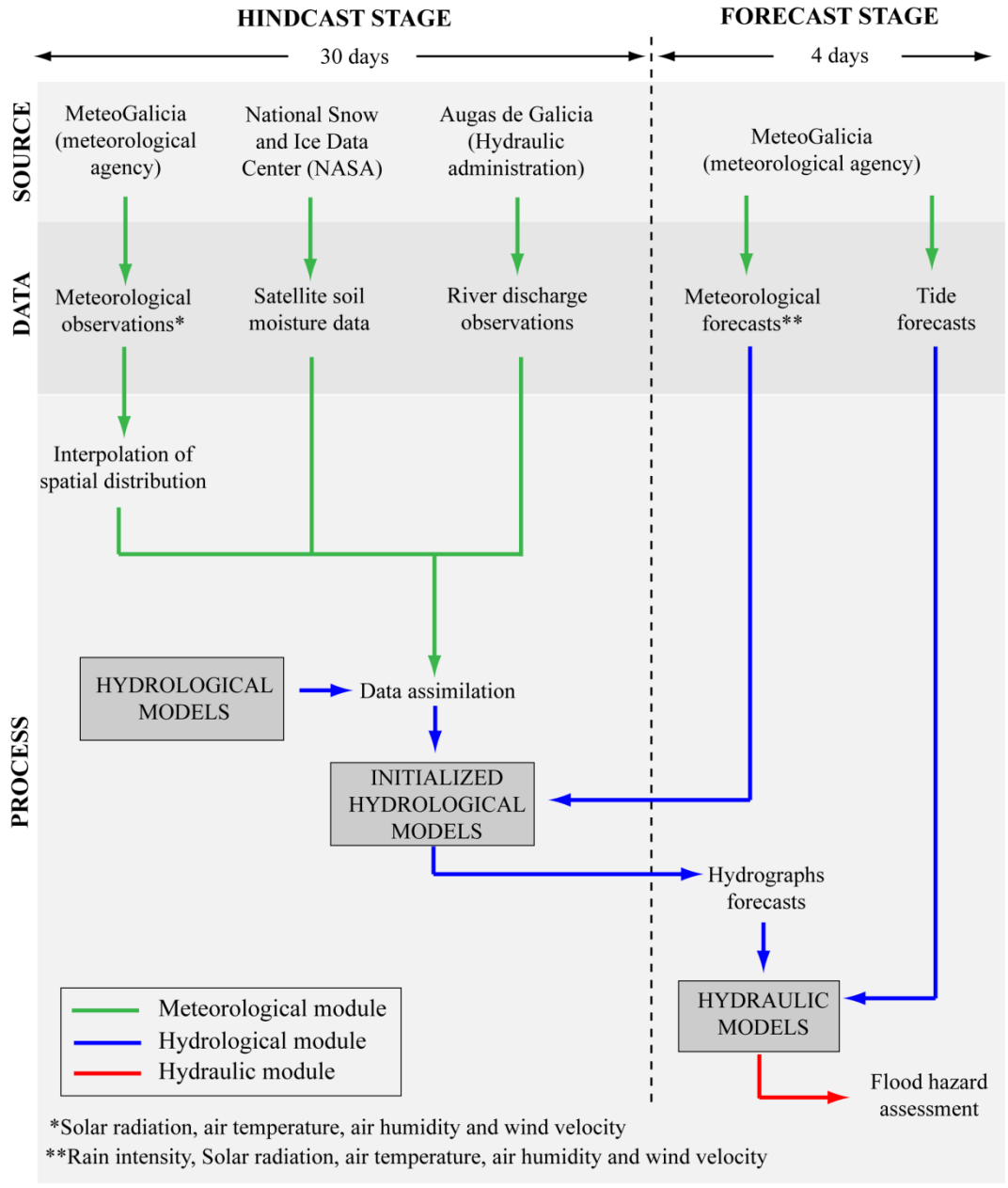

Figure 1. Flowchart of the MERLIN system showing the tasks performed by each module.

To perform these tasks, MERLIN is structured in three modules (meteorological, hydrologic, and hydraulic), orchestrated by a Python script. This script systematizes the operation of the system and performs the information exchange between the modules.

2.2. Meteorological module

The meteorological module acquires and processes the meteorological data used by the hydrological models during both the hindcast and forecast stages. The module also performs the conversion of all the generated outputs to the file formats required by the hydrological models.

2.2.1. Hindcast stage

During the hindcast stage, the observations processed are soil moisture, river discharge, rainfall, air temperature, wind speed, air moisture and solar radiation. Rainfall, air temperature, wind speed, air moisture and solar radiation data are obtained from the monitoring stations operated by MeteoGalicia, the regional weather agency. These variables are registered every 10 minutes. The spatial distribution of air temperature, wind speed, air moisture and solar radiation is interpolated from the values registered at the stations using the ordinary kriging (OK) technique (Goovaerts, 1997). Isotropic variograms obtained from hourly data of each variable are used in the interpolation. The resulting fields have a 1-hour temporal resolution, and a 1-km spatial resolution.

Rainfall fields are computed from rain gauge and meteorological radar observations, using the kriging with external drift (KED) technique (Haberlandt, 2007). The radar data operated by MeteoGalicia has spatial and temporal resolutions of 1 km and 5 minutes respectively, and covers the whole region of Galicia. Computing the rainfall fields using the KED technique instead of the OK improves the characterization of the spatial distribution of rainfall (Schiemann et al., 2011; Jewell and Gaussiat, 2015), since

it combines the advantages of the rain gauge measurements (high accuracy of rainfall data at ground level) and radar data (high space–time resolution of the observations). The accurate representation of the spatial variability of rainfall is particularly important in small catchments due to the significant impact on the performance of rainfall-runoff models (Emmanuel et al., 2015; Engeland et al., 2016, Cea and Fraga, 2018). The variogram used in the KED is obtained following the procedure described by Delrieu et al (2014). In case of missing radar data (due to radar breakdown, maintenance, etc.), the interpolation of the rainfall fields is performed using the OK technique, with a variogram obtained from the 10-minute rainfall depth measured at the rain gauges. No matter if rainfall is interpolated with KED or OK, the rain fields have a 10-minute temporal resolution, and a 1-km spatial resolution.

Soil moisture data corresponds to the products of the Soil Moisture Active Passive (SMAP) satellite provided by the National Snow and Ice Data Center. In particular, level 4 root-zone soil moisture data is used, which has spatial and temporal resolutions of 3 hours and 9 km respectively. The meteorological module acquires the root-zone moisture at the beginning of the hindcast stage and associates the moisture value of the closest pixel to each sub-basin of the hydrological models.

Discharge data is obtained from the stream gauge network operated by Augas de Galicia, the regional hydraulic administrator. The data are obtained from water level measurements performed every 10 minutes, converted to discharge values using previously calibrated rating curves.

2.2.2. Forecast stage

During the forecast stage, the meteorological module acquires the outputs of the Weather Research and Forecasting (WRF) model (Skamarock et al. 2005) operated by MeteoGalicia, that issues a daily 96-hour forecast. From the available predictions, the

system uses the rainfall, temperature, air humidity, solar radiation and wind speed forecasts, with temporal and spatial resolutions of 1 hour and 4 km respectively.

The meteorological module also acquires the tidal levels forecasted by the Regional Ocean Modelling System (ROMS) (Shchepetkin and McWilliams, 2005) at the catchment outlets. The ROMS setup for the Galician coast, operated by MeteoGalicia (Carracedo, 2003), include both astronomic and atmospheric tidal components, which are particularly relevant for predicting inundation events in coastal river reaches due to the interaction of sea level and river discharge (Acreman, 1994; Hawkes, 2003; Sopelana et al. 2018, Zhong et al. 2013). The forecasts of tidal levels are used as the boundary conditions of the 2D inundation models, as described in the following sections.

2.3. Hydrological module

The hydrological module forecasts the discharges along the catchments included in the forecasting system. This module consists of the hydrological models of the catchments included in the forecasting system, and several functions written in Python for launching the simulations and processing the model outputs.

2.3.1. Hydrological models

The hydrological model of each basin was built using the HEC-HMS Version 4.2.1 (Scharffenberg & Fleming, 2006), one of the most widely used models in hydrology. In addition, HEC-HMS is extensively used in operational systems due to its low computational burden and the numerous tools available for input and output data conversions. However, the modular structure of the MERLIN forecasting system makes it straightforward to replace the hydrologic and hydraulic models by any other models preferred by the user.

HEC-HMs is a semi-distributed model that discretizes the catchment in river reaches and sub-basins with spatially uniform properties. The formulations used to reproduce the simulated physical processes, and the required input parameters are shown in Table 1. Whereas certain parameters remain fixed during model set-up, others were tuned on a daily basis as explained in the following sections.

Physical process	**Formulation**	**Input parameters**
Rainfall interception	Dynamic canopy	Vegetation storage capacity (V_C)
Rainfall-runoff transformation	SCS unit hydrograph	Lag time (T_L)
Rainfall losses	Soil Moisture Account (SMA)	Percentage of initial soil water content and each groundwater layer (SM_S, SM_{GW1}, SM_{GW2})
		Soil Maximum infiltration rate, storage capacity, and percolation rate * (I_S, V_S, P_S)
		Storage, routing, and percolation coefficient for each groundwater layer *(V_{GW1}, R_{GW1}, P_{GW1}, V_{GW2}, R_{GW2}, P_{GW2})
Baseflow	Linear reservoir	Routing coefficient * (R_{GW1}, R_{GW2})
Flow routing	Kinematic wave	Manning coefficient
Evapotranspiration	Penman-Montheit	None

Table 1. Formulations and input parameters of the hydrological models. Parameters with * were tuned during the hindcast stage.

Rainfall interception by vegetation is simulated using the dynamic canopy formulation. According to this approach, vegetation is modelled as a deposit where a certain volume of rainfall can be retained (V_c). Stored water is lost by evapotranspiration, which is computed following the Penman-Montheit formulation using solar radiation, air temperature, air humidity and wind speed data. Rainfall exceeding the capacity of the deposit is conveyed to the surface, where it infiltrates and generates runoff (Figure 2).

Runoff hydrographs are computed using the SCS unit hydrograph method (Cronshey, 1986), requiring as input parameter the lag time of each sub-basin (T_L), defined as the delay between the peak rainfall intensity and the peak discharge. This time interval is computed from elevation and roughness data following the TR55 formulation

(Cronshey et al. 1985).

Rainfall infiltration is modeled using the Soil Moisture Account formulation (Bennet & Peters, 2000). This methodology discretizes the terrain in three deposits (Figure 2). One deposit represents the soil layer with a storage capacity of V_S. The other two represent underground layers with storage capacities of V_{GW1} and V_{GW2}. Rainfall infiltrates into the soil deposit at a rate computed from the maximum infiltration rate (I_S) and the moisture content of the soil layer (SM_S). Water stored in the soil deposit can be lost by evapotranspiration or percolate to shallower underground deposits. The percolation rate is computed from the maximum percolation rate (P_s), and the moisture content of the soil and shallow underground deposits (SM_S and SM_{GW1}). Water flowing into a shallow underground deposit can either percolate to the deepest deposit or flow to the river bed as interstitial flux. The percolation rate is computed from the maximum percolation (P_{GW1}) and the water content of both underground deposits (SM_{GW1} and SM_{GW2}). Interstitial flow is simulated using a linear reservoir model with conductivity R_{GW1}. Inflows into the deep underground deposit can either percolate to a deep aquifer, where they are stored indefinitely, or conveyed to the stream as interstitial flows.

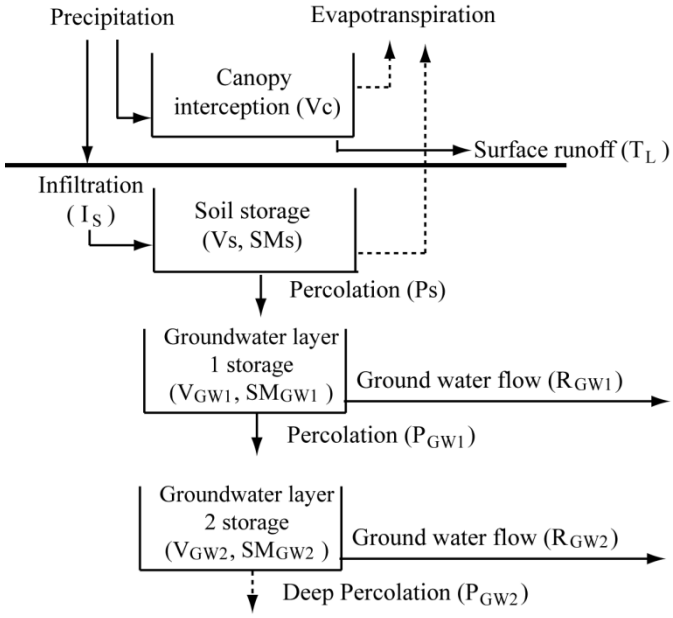

Figure 2. Flowchart of the water fluxes in the Soil Moisture Account formulation. Dashed lines represent processes that detract water from the system.

Runoff and interstitial flows conveyed to the stream are propagated following the kinematic wave formulation, which computes water velocity and depth from the slope and roughness (n_C) of river reaches.

2.3.2. Hindcast and forecast stage

During the hindcast stage, the hydrological model of each catchment assimilates observed discharge and meteorological data to reproduce the soil infiltration capacity at the beginning of the forecast stage. To this end, hydrological models are fed with the meteorological observations described in section 2.2.1, and the infiltration parameters are tuned to fit the computed discharges to the observed ones.

At each sub-basin, the moisture content of the soil and underground layers (SM_S, SM_{GW1} and SM_{GW2}) are obtained from SMAP satellite data. The remaining SMA parameters (I_S, V_S, P_S, V_{GW1}, R_{GW1}, P_{GW1}, V_{GW2}, R_{GW2}, and P_{GW2}) are calibrated to fit the observed discharges. To simplify the calibration procedure, the same value of each parameter is allocated to all the sub-basins of each catchment. A Nelder-Mead algorithm is used to search for the optimum parameter values, using the Nash-Suttcliffe Efficiency Index (NSE) as the objective function. The number of iterations is set to 100 in order to reduce the computational burden and allow an early delivery of the forecasting system. In order to improve the convergence of the hindcast process, the values of the input parameters of each catchment obtained for the previous day are used as seed values.

During the forecast stage, hydrological models predict the discharges along the studied catchments for the upcoming 4 days. For this purpose, the models are fed with the meteorological forecasts described in section 2.2.2 and the parameter values obtained

from the hindcast stage. By doing so, the hydrological models accurately reproduce the infiltration capacity of the catchment during the simulated period.

2.4. Hydraulic module

The hydraulic module computes the flood extent from the discharges forecasted by the hydrological module and the tidal level forecasts. The hydraulic module comprises the hydraulic models of the flood prone areas of the catchments included in the forecasting system. Moreover, the module includes a set of python functions used to set the corresponding boundary conditions of the hydraulic models, launch the simulations, and process the outputs.

2.4.1. Hydraulic models

The hydraulic models used in the MERLIN forecasting system are Iber+ models (García-Feal et al. 2018), a GPU parallelized version of the Iber model (Bladé et al. 2014). Iber solves the two-dimensional shallow water equations over both structured and unstructured meshes, using a finite volume approach. The Iber model has been validated in many previous studies (Bermúdez et al. 2017; Cea and Bladé, 2015; Cea and French, 2012; Fraga et al. 2017), and it has proved to deal efficiently with some of the main numerical difficulties that appear in the modelling of overland flow, such as the presence of highly unsteady wet–dry fronts, small water depths, and high bed friction (Cea and Bladé, 2015). The parallelized version of the model decreases in two orders of magnitude the computational time, which is especially relevant for flood forecasting since flood warnings have to be delivered as soon as possible.

Unlike hydrological models, hydraulic models do not require initialization and therefore run only during the forecast stage. The input parameters required by hydraulic models are the roughness coefficients defined during model set-up.

For each day of the forecast stage, the hydraulic models are run using as boundary conditions the discharge and tidal levels forecasted for the referred day. This approach is adapted for coastal river reaches, where flood extent is conditioned by both fluvial discharges and the tidal level. The computed flood hazard and maximum water depths are interpolated to raster files. These rasters are plotted over geo-referenced photographs, showing the time stamp corresponding to maximum flooding (Figure 3). The generated images and the forecasted hydrographs can be sent to local stakeholders, who can use this information to alert the population, and to activate evacuation and defence protocols. In addition, the time series of the water depths at control points are extracted to compare the computed values against measured data when available.

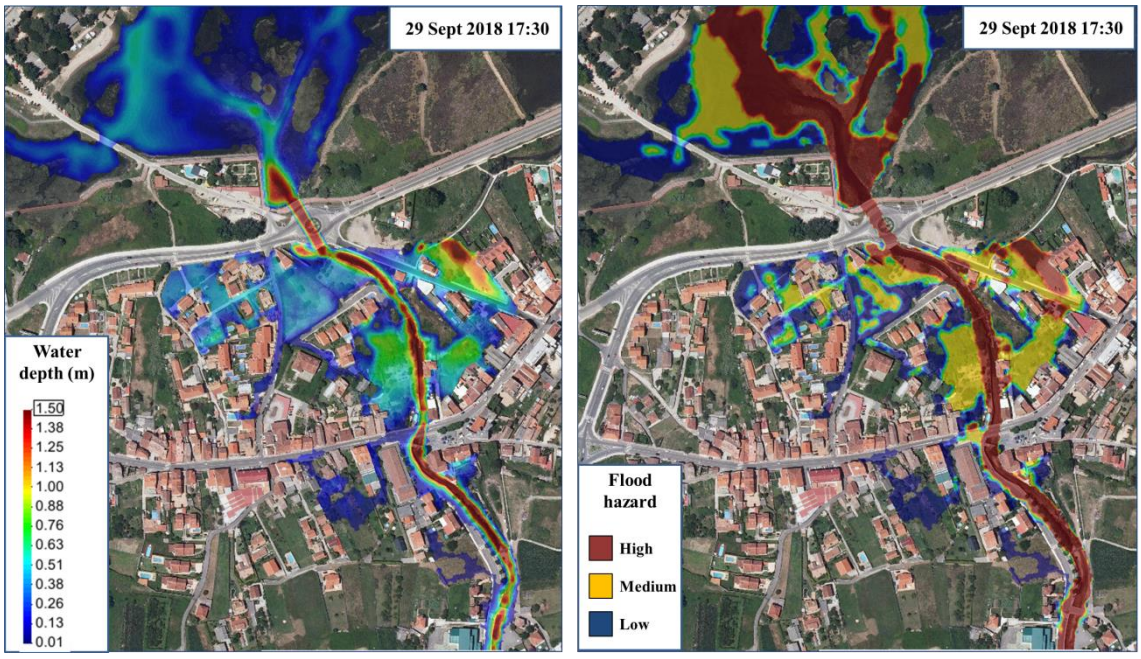

Figure 3. Example of hydraulic model output at one of the catchments described in section 3. Flood hazard was determined in accordance with Spanish legislation.

2.4.2. Triggering of the hydraulic model simulations

In order to save computational resources, the hydrodynamic simulations of the flood prone areas are run only when forecasted discharges are expected to cause flooding. For this purpose, discharges predicted by the hydrological models are compared against the

bankfull discharges. This comparison is performed separately for each catchment and each day of the forecast stage (Figure 4). When forecasted discharges are higher than the bankfull discharges, the watercourse capacity is exceeded. In this case, the simulation of the hydraulic model is launched to compute the inundation extent and flood hazard.

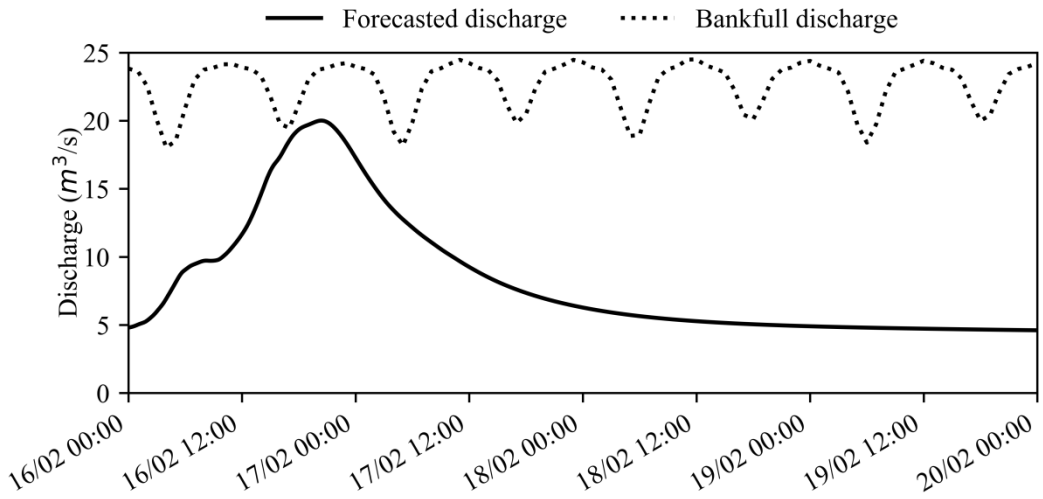

Figure 4. Example of flood risk and maximum waterway capacity forecasts at one of the catchments.

The bankfull discharge of each river reach was determined prior to the forecast system set up. To this end, the hydrodynamic models of the flood prone areas were used. Multiple simulations were run for every model, each with a fixed tidal level at the basin outlet and a slowly increasing discharge at the inlet boundary. For each simulation, the bankfull discharge was considered as the maximum discharge flowing without exceeding the waterway at any point of the river reach. It is important to remark that no specific location was selected a priori to define the bankfull discharge. From the results of the hydrodynamic simulations, the river cross-section where overflow first occurred was identified, and the bankfull discharge was defined as the discharge flowing through that section just before the waterway capacity was exceeded. If an overflow occurred far from the river mouth, where the flow is not influenced by the tide, the bankfull discharge will be the same for any tidal level. However, in the catchments included in

the MERLIN forecasting system, overflow started near the river mouth, so the maximum discharge depended on the tidal level. The bankfull discharges and tidal levels obtained at each catchment during the described simulations were fitted to a curve (Figure 5). These curves and the tidal level forecasts described in section 2.2.2 were used to estimate the bankfull discharges over the upcoming days (Figure 4).

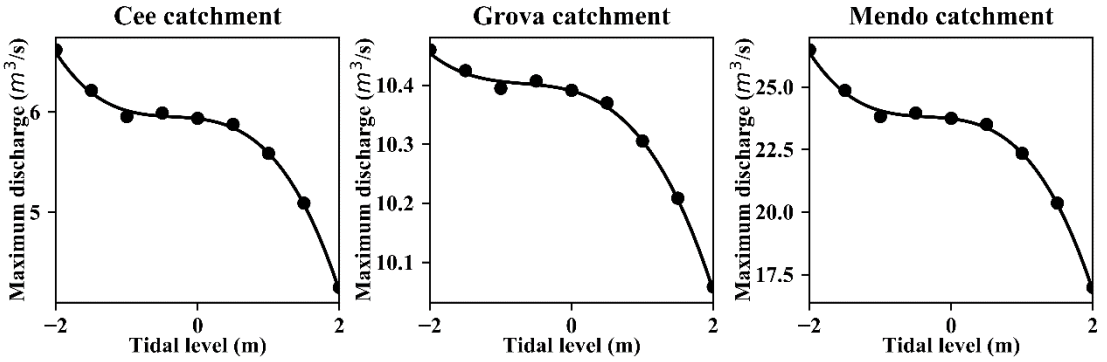

Figure 5. Relation between bankfull discharge and tidal level for the catchments described in section 3. Dots correspond to the values obtained for each simulation and the solid line to the fitted curve.

3. System implementation

This section reviews the application of the MERLIN system for forecasting the flood hazard in three areas located in coastal catchments in north-western Spain. The MERLIN system run on an Intel Core i7 7700 3.6 GHz CPU, with 32 GB of RAM, and a NVIDIA Gforce GT730 GPU. The time required to perform the whole forecasting process, which included both the hindcast and forecast stages of the three catchments, was approximately 1 hour.

3.1. Catchments description

The flood hazard forecasting system was implemented in three coastal catchments in the northwest of Spain. The studied catchments are those of the rivers Cee, Grova and Mendo (Figure 6). In the three catchments there are urbanized areas exposed to flood risk. These are the towns of Cee, Baiona and Betanzos, with populations of around 8000, 12000 and 13000 inhabitants respectively.

The studied catchments present similar characteristics in terms of land use and topography (Table 2). However, they differ in size and lag times. The lag times were determined by analysing the hydrographs computed by the hydrological model of each catchment when constant rain intensity was imposed. Discharge data from the monitoring network operated by Augas de Galicia was available near the outlet of each catchment. The Annual Exceedance Probability Discharges (AEP) presented in Table 2 were obtained from Augas de Galicia (2016).

	Catchment Area (Km^2)	Q_F (m^3/s)	Catchment Land use (%)			River length (km)	Maximum height (m.a.s.l)	T_L (hours)
			Forest	Agricultural	Moors			
Cee	4.95	3.1	28	42	30	4.7	300	0:50
Grova	16.96	14.0	27	27	46	9.7	650	1:20
Mendo	83.9	60.31	26	66	8	32.2	500	4:30

Table 2. Characteristics of the three catchments. T_L corresponds to the lag time of the catchment, and Q_F to the 1 / 3 AEP discharge

The catchments are located in the region of Galicia, which is situated in the path of incoming low pressure fronts from the Atlantic Ocean. These fronts are generated in polar regions and move southeast with the prevailing winds. The incoming fronts are uplifted at the coastline due to the steep terrain of the coastal region, which generates adverse weather events with intense rainfalls characterized by high spatial and temporal variability (Cabalar- Fuentes, 2005). This behaviour is also observed in other regions, such as the U.S. Pacific Coast, given the similar latitude and orography (Eiras- Barca, Brands, & Miguez- Macho, 2016).

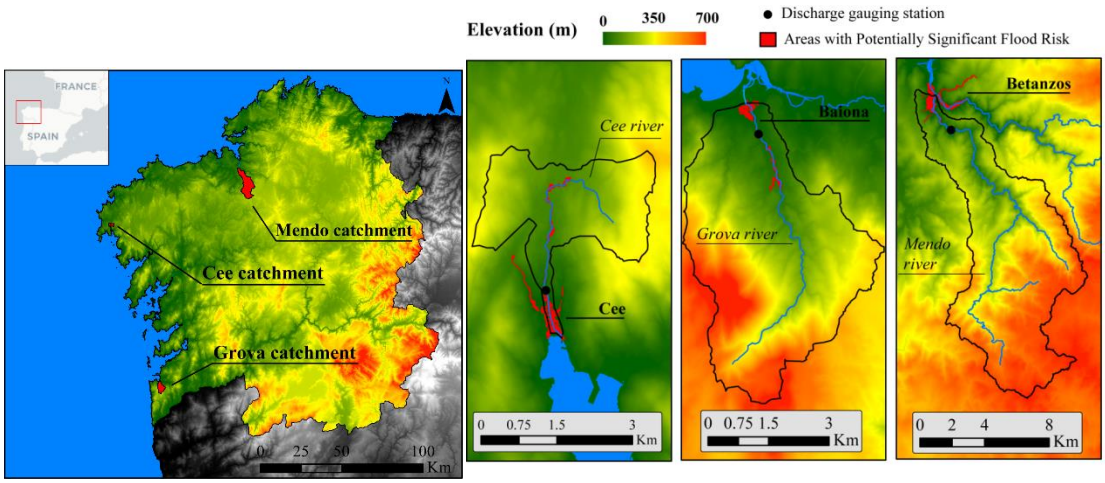

Figure 6. Location and topography of the Cee, Grova and Mendo catchments used to analyse the performance of the MERLIN system.

3.2. Hydrological model set-up

The hydrological model of each catchment was built using the HEC-GeoHMS software (Fleming & Doan, 2009). Elevation data from a 5 meters Digital Elevation Model (DEM), provided by the Spanish National Geographical Institute, was used to define the extent and slope of the sub-basins and river reaches (Table 3). Land use data obtained from the Corine Land Cover service was used to compute the amount of impervious surface and the roughness coefficient for each sub-basin. The Manning coefficients of all the river reaches were set to 0.06 $s.m^{-1/3}$ after visual inspections. The vegetation storage capacity of the sub-basins (V_C in Table 1) was set to 2 mm. This value was selected from the range recommended in the HEC-HMS user's manual, taking into account land use. The same value was allocated to the sub-basins of the three catchments, since all of them have a similar percentage of forested areas.

3.3. Hydraulic model set-up

The hydraulic model of each catchment covers the Area with Potential Significant Flood Risk (APSFR) of the basin, as defined by the Flood Risk Management Plan of Galicia-Costa 2015–2021 (Inungal, 2016). Models also extend the estuary downstream

the river mouth to include the tidal level forecasts as boundary conditions (Figure 7). The computational meshes were built to ensure an accurate discretization of each domain while avoiding a large number of elements. These premises become crucial towards achieving good model performance in affordable computational times (Costabile et al. 2011; Costabile & Macchione, 2015). To this end, the discretization of the APSFR areas was performed using the IberGUI. This tool allows combining structured and un-structured meshes, resulting in a more efficient discretization of the domain.

The river channels were discretized in structured meshes with element sizes of 2 meters. The rest of the domain was discretized in un-structured meshes with coarser resolutions to reduce the number of elements of the meshes (Table 3). In urbanized areas, buildings were modelled as holes in the computational mesh. The element size was set to 3 meters to accurately reproduce the topography of streets and pathways. River estuaries were discretized using larger elements (Figure 7), using mesh elements of size 30, 20, and 60 m at the Cee, Grova, and Mendo models respectively. The reason for this was that estuaries were included mainly to simulate the tidal level near the river mouth. A detailed characterization of the hydrodynamics at the estuary was not required to compute the flood extent in urbanized areas. Therefore, they were discretized into larger elements in order to reduce the computational burden.

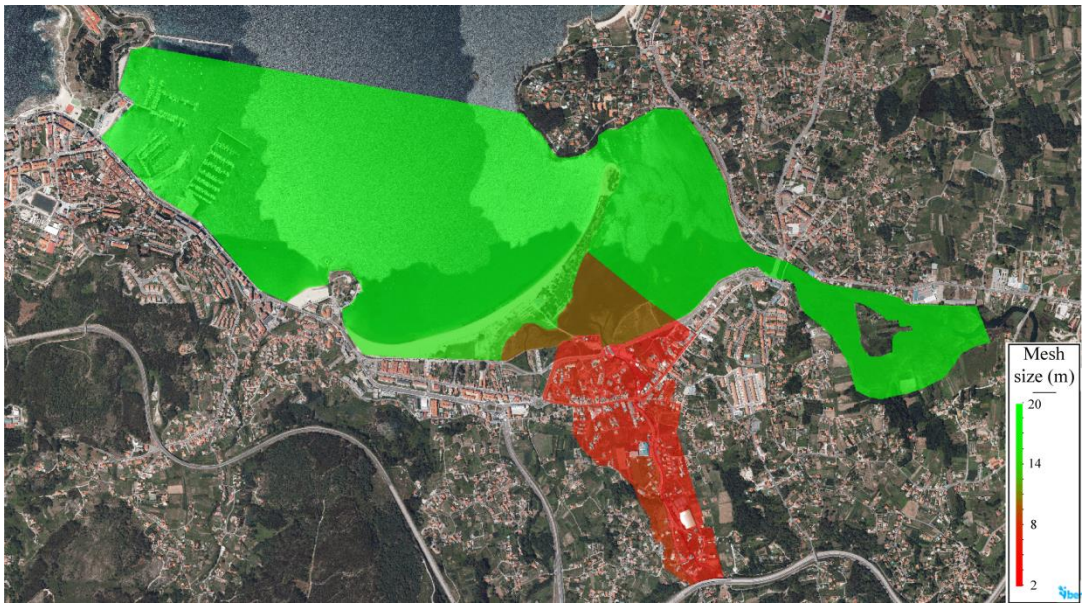

Figure 7. Element size distribution in the hydraulic model of the Grova catchment.

Elevation data was obtained from 1 m resolution DEM produced by the Spanish National Grographical Institute. The roughness coefficient of each element was set from the corresponding land use and the values recommended in the Iber user's manual. Land use was defined from visual inspections and aerial photography of the catchments.

	Hydrological model		Hydraulic model		
Basin	Number of sub-basins	Sub-basin size range (km^2)	Model area (m^2)	Number of elements	Element size range (m)
Cee	7	0.48-1.22	552115	29474	2 - 30
Grova	18	0.36– 2.80	2720417	32944	2 - 20
Mendo	23	0.79-6.90	8173792	136582	1.5 - 60

Table 3.Main characteristics of the hydrological and hydraulic models.

4. Results and discussion

4.1. Results

The performance of the MERLIN system in the 3 catchments described in section 3 was

evaluated over 4 months spanning over winter and spring. An example of the discharge forecasts produced by the flood forecasting system on a daily basis is shown in Figure 8, where observed discharges and rainfall were added a *posteriori* to evaluate the accuracy of the predictions. At the Mendo catchment, despite small deviations observed in the shapes of the rising and recession limbs of the hydrograph, peak discharges were correctly predicted both in terms of magnitude and time. However, since meteorological forecasts over predict rainfall, the total runoff volume was over estimated. The results at the Cee and Grova catchments are presented as an example of the importance of rain forecasts in the performance of the warning system. At the Cee catchment, peak rain intensity was underestimated, causing under-prediction of forecasted discharges. In contrast, the meteorological forecasts at the Grova catchment overestimated maximum rain intensity, so predicted discharges exceeded the observed ones at the peak of the hydrograph.

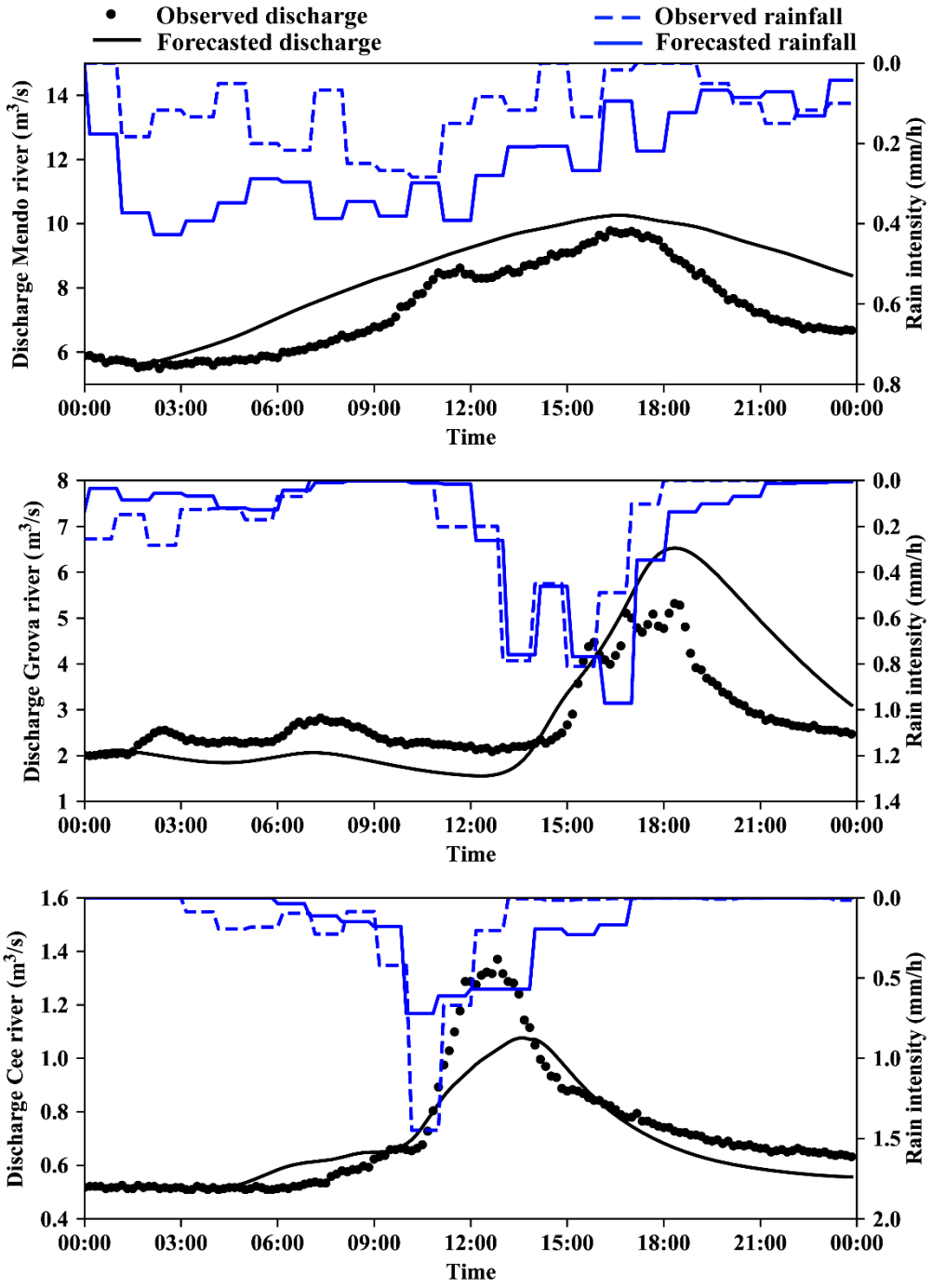

Figure 8. Example of the discharge forecasts and observations.

The accuracy of the forecasts delivered by the MERLIN system during the whole evaluation period is shown in Figure 9, where rain intensities correspond to a 10-minute interval and were measured at rain gauges located inside the Cee catchment, approximately 10 km northeast from the Grova catchment and around 15 km east from the Mendo basin.

The degree of collinearity between simulated and measured discharges is quantified using the coefficients of determination R^2. The R^2 coefficients 0.81, 0.68, and 0.39 are obtained at the Mendo, Grova and Cee catchments. It is important to remark that the R^2 values are remarkably higher than those obtained for the peak rain intensities at the Mendo (0.47), Grova (0.2) and Cee (0.27) catchments. The percent bias (PBIAS) of the forecasted discharges, which measures the average tendency of the simulated values to be larger or smaller than the observations, indicate that peak discharges were under predicted at the Mendo and Grova catchments, and over predicted at the Cee catchment.

At the three catchments, the R^2 coefficients between the forecasted and observed water depths are similar to the R^2 coefficients between the predicted and measured discharges. In contrast, the PBIAS decrease significantly in magnitude, especially at the Cee and Grova catchments. Differences between predicted and observed water depths are below 10% in most cases, which represent errors of about 10-15 cm. Furthermore, it is likely that these errors could be further reduced since they can be partially explained by the discretization of the river reach. Hydraulic models with finer resolutions would capture more precisely the elevation of the river bed at the gauging sections, which would improve the accuracy of water level forecasts. However, this would increase the computational cost of the system, which could limit its ability to deliver early flood warnings. This is particularly relevant since water depths, rather than discharges, determine the flood extent.

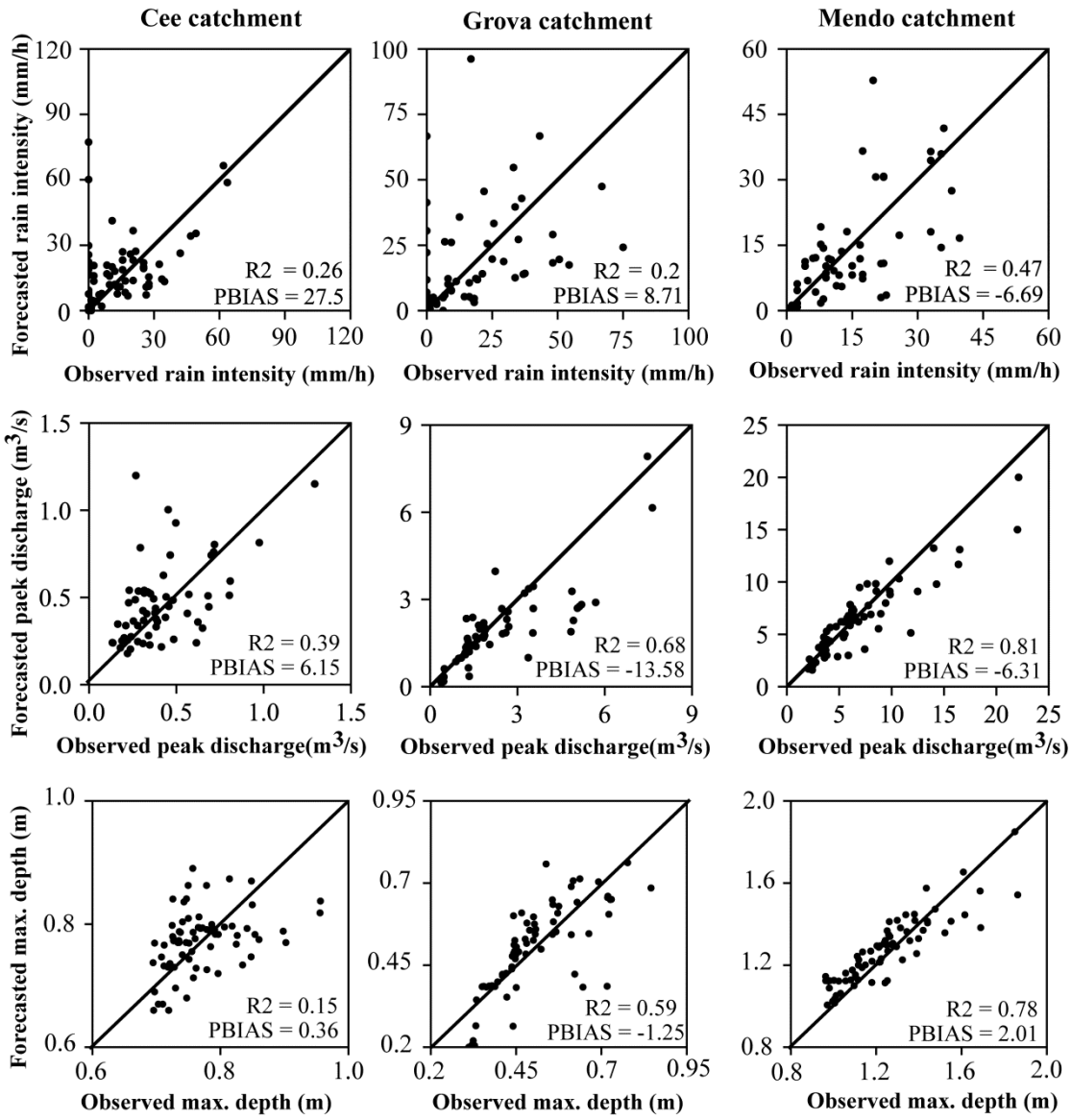

Figure 9. Comparison between observed and forecasted values. Rain intensities correspond to a 10-minute interval. Predicted values correspond to 24-hour forecasts.

Results presented in Figure 9 correspond to forecasts for the upcoming day. Figure 10 shows the comparison between the measured and forecasted peak discharges for different time horizons. At the Mendo and Grova catchments, results show an increase in the accuracy of forecasted discharges as the time horizon decreases, as measured by the relative mean square errors (RMSE). At the Mendo catchment, the RMSE of the discharges forecasted for one day in advance (2 m^3/s) halves those corresponding to forecasts performed with four days in advance (4.14 m^3/s). At the Cee catchment, no improvement in the accuracy of discharge forecasts is observed.

At the three studied catchments, the sign for the PBIAS remains constant regardless of the time horizon of the forecast. Discharges forecasted at the Mendo, and Cee catchments present a relative constant PBIAS. At the Grova catchment, PBIAS vary depending on the antecedent days of the forecast.

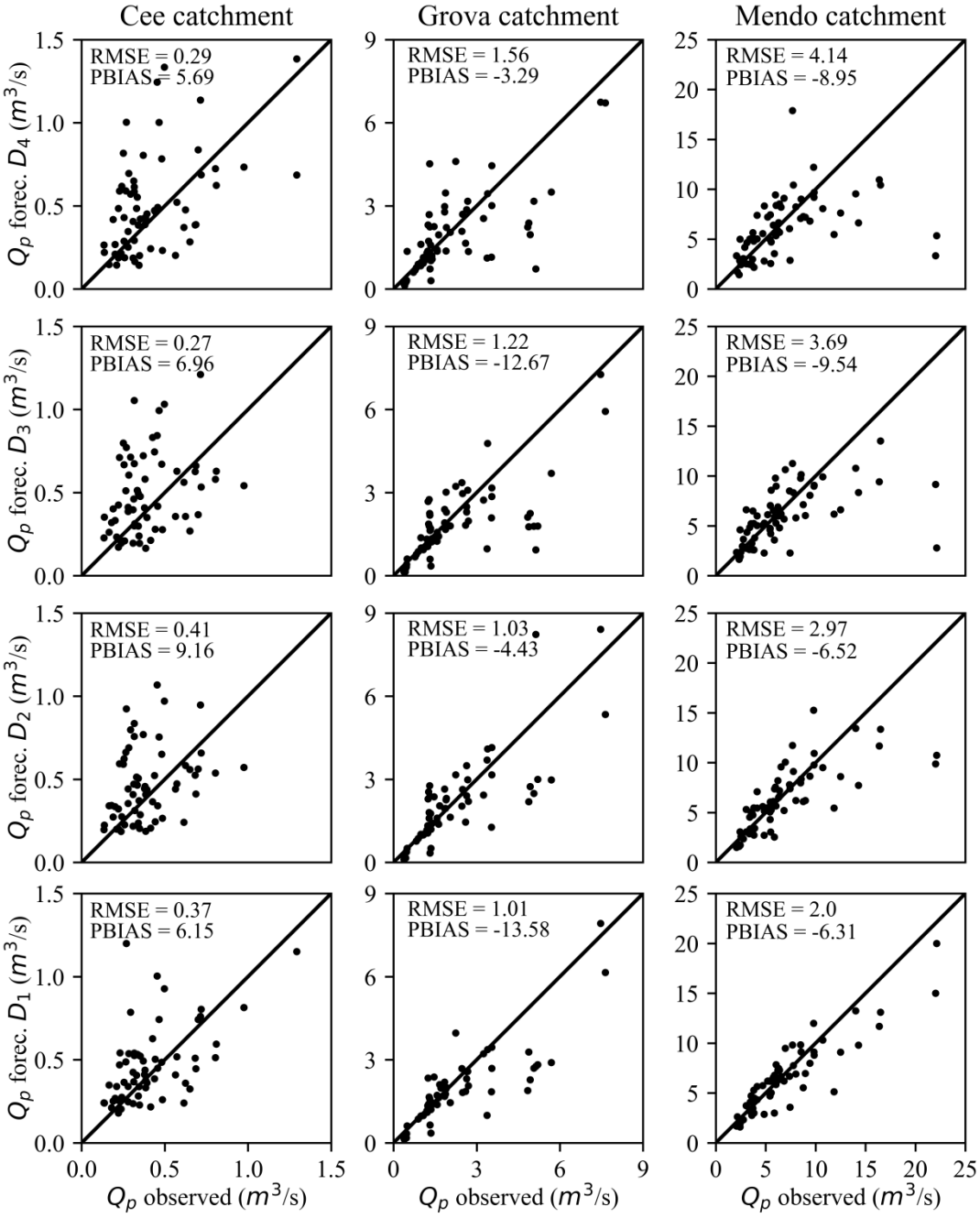

Figure 10. Comparison between observed and forecasted peak discharges with different days in advance (D1 to D4). Solid black line corresponds to a 1:1 line

4.2. Discussion

The results presented substantiate the adequate performance of the MERLIN flood forecasting system during the evaluation period. The RMSE and R^2 coefficients obtained for the forecasted discharges and water levels are acceptable (according to Moriasi et al., 2007), especially in the Mendo and Grova catchments. In addition, the PBIAS of the forecasted discharges at the three catchments are similar to the values reported for other flood forecasting systems (Neto et al., 2104; Laminchane and Sharma, 2017; Abdullah et al. 2018).

It is worth noting that the R^2 coefficients of the predicted discharges are higher than the R^2 coefficients of the predicted rainfall at the three catchments. This implies that the meteorological forecast errors are attenuated during the rainfall runoff computations. In addition, the accuracy of the forecasting system increases when discharge forecasts are converted to water levels by the hydraulic models, which may be inferred from the decrease in the PBIAS shown in Figure 9.

The R^2 coefficients between the observed and forecasted discharges increase with the size of the catchment. For the Mendo catchment (83.9 km^2), the R^2 coefficient of the forecasted discharges doubles the R^2 coefficient of the Cee basin (4.95 km^2). In small catchments, small deviations in the storm path forecasted can significantly vary the average rainfall depth in the whole basin, leading to significant differences in the computed discharges. In comparison, bigger catchments are less sensitive to small deviations in the storm path since due to their large surface and rainfall is still likely to fall within the catchment.

The least accurate predictions of peak discharge are obtained in the Cee catchment, where the system systematically over predicts the observed discharge (positive PBIAS).

This is partially explained by the high and positive PBIAS of the rain intensities forecasted in this catchment (Figure 9), which indicate that rainfall tends to be overestimated. A plausible explanation is the location of the Cee catchment in the western coast of Galicia (Figure 6), where most storms arrive from the Atlantic Ocean. The uplift of the low pressure fronts occurring when the fronts hit the coast hinders the accuracy of meteorological forecasts. This fact may also explain the low R^2 coefficients of the predicted rainfall at the Grova and Cee catchments (0.26 and 0.20), which are much lower than the R^2 coefficient at the Mendo catchment (0.46), located on the northern coast. In fact, high rainfall intensities were forecasted for several days in the Cee and Grova catchments, although no rainfall finally occurred. In addition, the fact that the catchment is crossed by several roads and infrastructure that were not explicitly represented in the hydrological model, might have had an effect on performance of the model, especially given the small size of the catchment. Moreover, the narrow width of the stream network makes it difficult to accurately represent low flows in the hydrologic and hydraulic models, which are those that mainly occurred during the evaluation period of the system. It should be noted that the R^2 coefficient in the Cee catchment is much lower for the water level than for the discharge, whilst the Grova and Mendo water levels and discharges obtained similar R^2 values as shown in Figure 9. This indicates that there is a source of uncertainty in the transformation of the water discharges to water levels in the Cee catchment. This uncertainty should be addressed with a more accurate representation of the stream network and infrastructures, both in the hydrological and hydraulic models (Costabile and Macchione, 2015).

The performance of the NWP model may also explain the increase of the accuracy in the predicted discharges at the Grova and Mendo catchments as the time horizon diminishes. The hydrological response of larger catchments is related to large-scale

atmospheric processes, which are better predicted by the meteorological models for short lead times (Gimeno et al. 2014). However, the ability of NWP models to capture small scale atmospheric processes that explain the hydrologic response of small catchments is still limited nowadays, regardless of the lead time (Wick et al. 2013).

The previous findings underscore the need for quantifying uncertainty in the prediction chain (from rainfall through discharge to water levels), in order to estimate the reliability of flood hazard warnings. This is not a straightforward task since there are many sources of uncertainty, including rainfall input data (Fraga et al. 2018; Moulin et al. 2009; Villarini et al. 2008), the initialization of the hydrological model before each rainfall event (infiltration parameters), the calibration of the hydrological and hydraulic models (Beven and Binley, 2014; Huard and Mailhot, 2006; Lehbab- Boukezzi et al. 2016), and the formulations used to model the hydrological and hydraulic processes, also known as model structural uncertainty (Beven and Binley, 2014).

Finally, it is important to remark that the results obtained in this study correspond to a four-month evaluation period. During this period, the maximum observed discharges were approximately 1/3 of the mean annual maximum discharge. Therefore, further insight into the performance of the system during intense flood events is still required.

5. Conclusions

This paper presents MERLIN, a new flood hazard forecasting system for coastal river reaches located in small and medium-size catchments. In order to account for the antecedent moisture content of the soil, the system operates in two stages. First, the system hindcasts the infiltration capacity of soil using meteorological and discharge observations. Then, the flood hydrographs and inundation hazard along flood prone areas are computed from meteorological forecasts. The system considers the joint

effects of tidal level and river discharge in the computation of the inundation hazard, and exploits recent improvements in High Performance Computing techniques applied to inundation models that enabled high-resolution two-dimensional simulations in relatively short time lapses.

The performance of the forecast system was analysed during a few months period in winter and spring, with good performance being obtained for lead times of 24 to 48 hours. Predictions improve as the size of the catchment increases. For larger time horizons the predictions deteriorate mainly due to the poor quality of the precipitation forecasts. Though the preliminary work presented in this study should be corroborated with further data gathered during future flood events, the system has proven to be potentially useful.

Finally, it is important to remark that unexpected flooding may cause substantial damage and even the loss of human lives; hence, the design of flood warning systems should be conservative, since the consequences of under-prediction were far more serious than those of over-prediction.

6. References

Abdullah J, Muhammad NS, Julien P. Y, Ariffin J, Shafie A. (2018). Flood flow simulations and return period calculation for the Kota Tinggi watershed Malaysia. J. Flood Risk Manag, 11 S766-S782.

Acreman M.C. (1994) Assessing the joint probability of fluvial and tidal floods in the river-roding. J Inst Water Environ Manag, 8 490–496.

Aguas de Galicia (2016). Anexo 1 Caracterización das ARPSIS. In Plan de Xestión do Risco de Inundación da Demarcación Hidrográfica de Galicia-Costa (ciclo 2015–2021) Official Journal.

Alvarez-Garreton C, Ryu D, Western AW, Su CH, Crow WT, Robertson E, Leahy C (2015). Improving operational flood ensemble prediction by the assimilation of satellite soil moisture: Comparison between lumped and semi-distributed schemes. Hydrol. Earth Syst. Sci, 19(4) 1659-1676.

Arnell NW, Gosling SN (2016). The impacts of climate change on river flood risk at the

global scale. Clim. Change, 134(3), 387-401.

Bennett TH, Peters JC. (2000). Continuous soil moisture accounting in the hydrologic Engineering Center Hydrologic Modeling System (HEC-HMS). Building Partnerships. 1-10.

Bermúdez M, Neal J.C, Bates P.D, Coxon G, Freer J.E, Cea L. Puertas J. (2017). Quantifying local rainfall dynamics and uncertain boundary conditions into a nested regional- local flood modeling system. Water Resour. Res, 53(4) 2770-2785.

Beven K., Binley A. (2014). GLUE: 20 years on. Hydrological processes, 28(24), 5897-5918.

Bladé E, Cea L, Corestein G, Escolano E, Puertas J, Vázquez-Cendón E, Dolz J. Coll A. (2014). Iber: herramienta de simulación numérica del flujo en ríos. Rev. Int. Metod. Numer, 30(1) 1-10.

Brocca L, Moramarco T, Melone F, Wagner W, Hasenauer S, Hahn S (2011). Assimilation of surface-and root-zone ASCAT soil moisture products into rainfall–runoff modeling. IEEE Trans Geosci Remote Sens 50(7) 2542-2555.

Bhuiyan H, McNairn H, Powers J, Merzouki A (2017). Application of HEC-HMS in a cold region watershed and use of RADARSAT-2 soil moisture in initializing the model. Hydrol. 4(1) 9.

Cabalar- Fuentes M. (2005). Los temporales de lluvia y viento en Galicia. Propuesta de clasificación y análisis de tendencias (1961- 2001). Investigaciones Geográficas (Esp) 36.

Carracedo P. (2003). Acoplamiento de un modelo hidrodinámico de escala global con uno de escala regional para Galicia. Revista Real Academia Galega de Ciencias 22 85.

Cea L, French J. R. (2012). Bathymetric error estimation for the calibration and validation of estuarine hydrodynamic models. Est. Coastal Shelf Sci, 100 124-132.

Cea L. Bladé E. (2015). A simple and efficient unstructured finite volume scheme for solving the shallow water equations in overland flow applications. Water Resour. Res, 51(7) 5464-5486

Cea L, Fraga I. (2018). Incorporating antecedent moisture conditions and intraevent variability of rainfall on flood frequency analysis in poorly gauged basins. Water Resour. Res, 54 8774-8791.

Cools J, Vanderkimpen P, Afandi GE, Abdelkhalek A, Fockedey S, Sammany ME, Abdallah G, El Bihery M, Bauwens W, Huygens M (2012). An early warning system for flash floods in hyper-arid Egypt. Nat. Hazards Earth Syst. Sci, 12(2), 443-457.

Costabile P, Costanzo C, Macchione F (2011). Comparative analysis of overland flow models using finite volume schemes. J. Hydroinform. 14(1) 122-135.

Costabile P, Macchione F (2015). Enhancing river model set-up for 2-D dynamic flood modelling. Environ. Modell. Softw 67, 89-107.

Cronshey R. (1986). Urban hydrology for small watersheds. US Dept. of Agriculture Soil Conservation Service Engineering Division.

Cronshey R. G, Roberts R. T, Miller N. (1985). Urban hydrology for small watersheds (TR-55 Rev.). In Hydraulics and Hydrology in the Small Computer Age (pp. 1268-1273). ASCE.

Delrieu G, Wijbrans A, Boudevillain B, Faure D, Bonnifait L, Kirstetter P. E. (2014). Geostatistical radar–raingauge merging: A novel method for the quantification of rain estimation accuracy. Adv. Water Resour, 71 110-124.

Djordjevic S, Butler D, Gourbesville P, Mark O, Pasche E (2011). New policies to deal with climate change and other drivers impacting on resilience to flooding in urban areas: the CORFU approach. Environ Sci Policy, 14, 864 – 873.

Ehret U, Götzinger J, Bárdossy A, Pegram GG (2008). Radar- based flood forecasting in small catchments exemplified by the Goldersbach catchment Germany. Int. J. River Basin Manage. 6(4) 323-329.

Eiras- Barca J, Brands S, Miguez- Macho G. (2016). Seasonal variations in North Atlantic atmospheric river activity and associations with anomalous precipitation over the Iberian Atlantic Margin. J Geophys Res Atmos 121(2) 931–948.

Emmanuel I, Andrieu H, Leblois E, Janey N, Payrastre O. (2015). Influence of rainfall spatial variability on rainfall–runoff modelling: Benefit of a simulation approach?.J. Hydrol, 531 337-348.

Engeland K, Steinsland I, Johansen SS, Petersen-Øverleir A, Kolberg S. (2016). Effects of uncertainties in hydrological modelling. A case study of a mountainous catchment in Southern Norway. J Hydrol, 536 147-160.

Fleming MJ, Doan JH. (2009). HEC-GeoHMS geospatial hydrologic modelling extension: User's manual version 4.2. US Army Corps of Engineers Institute for Water Resources Hydrologic Engineering Centre Davis CA.

Fraga, I., Cea, L., Puertas, J. (2019). Effect of rainfall uncertainty on the performance of physically-based rainfall-runoff models. Hydrological Processes. 33, 160-173.

Fraga I. (2018). Analysis of the Effect of Tidal Level on the Discharge Capacity of Two Urban Rivers Using Bidimensional Numerical Modelling. MDPI Proceedings 2(18) 1175.

García-Feal O, González-Cao J, Gómez-Gesteira M, Cea L, Domínguez J, Formella A. (2018). An accelerated tool for flood modelling based on Iber. Water 10(10) 1459.

Givati A, Gochis D, Rummler T, Kunstmann H (2016). Comparing one-way and two-way coupled hydrometeorological forecasting systems for flood forecasting in the Mediterranean region. Hydrology, 3(2) 19.Goovaerts P. (1997). Geostatistics for Natural Resource Evaluation. Oxford University Press Oxford

Gimeno L, Nieto R, Vázquez M, Lavers DA. (2014). Atmospheric rivers: A mini-review. Front. Earth Sci, 2 2-10.

Haberlandt U, (2007). Geostatistical interpolation of hourly precipitation from rain gauges and radar for a large-scale extreme rainfall event. J. Hydrol. 332(1) 144-157.

Hawkes P.J. (2003) Extreme water levels in estuaries and rivers. The combined influence of tides river flows and waves. DEFRA Defra/Environment Agency. R&D Technical Report FD0206/TR1. HR Wallingford Report SR 645

Horita FE, Vilela R, Martins R, Bressiani D, Palma G, de Albuquerque JP (2018). Determining flooded areas using crowd sensing data and weather radar precipitation: a case study in Brazil. In ISCRAM.

Hossain F, Siddique-E-Akbor AHM, Yigzaw W, Shah-Newaz S, Hossain M, Mazumder LC, Turk FJ.(2014). Crossing the "valley of death": lessons learned from implementing an operational satellite-based flood forecasting system. Bull. Amer. Meteor. Soc, 95(8) 1201-1207.

Huard D., Mailhot A. (2006). A Bayesian perspective on input uncertainty in model calibration: Application to hydrological model "abc". Water Resources Research, 42(7), W07416

IPCC (2018). Global warming of 1.5°C. An IPCC Special Report on the impacts of global warming of 1.5°C above pre-industrial levels and related global greenhouse gas emission pathways in the context of strengthening the global response to the threat of climate change sustainable development and efforts to eradicate poverty. In Press.

Jewell S. A, Gaussiat N. (2015). An assessment of kriging- based rain- gauge–radar merging techniques. Q. J. R. Meteorol. Soc, 141(691) 2300-2313.

Kasiviswanathan KS, He J, Sudheer KP, Tay JH. (2016). Potential application of wavelet neural network ensemble to forecast streamflow for flood management. J. Hydrol, 536 161-173.

Kellens W, Vanneuville W, Verfaillie E, Meire E, Deckers P, De Maeyer P. (2013). Flood risk management in Flanders: past developments and future challenges. Water Resour. Manag 27(10) 3585-3606.

Krajewski WF, Ceynar D, Demir I, Goska R, Kruger A, Langel C, Small SJ (2017). Real-time flood forecasting and information system for the state of Iowa. Bull. Amer. Meteor. Soc. 98(3) 539-554

Kumar M, Sahay RR. (2018). Wavelet-genetic programming conjunction model for flood forecasting in rivers. Hydrol. Res, 49(6) 1880-188.

Lamichhane N, Sharma S. (2017). Development of flood warning system and flood inundation mapping using field survey and LiDAR data for the Grand River near the city of Painesville Ohio. Hydrol, 4(2) 24.

Lehbab- Boukezzi Z., Boukezzi L., & Errih M. (2016). Uncertainty analysis of HEC-HMS model using the GLUE method for flash flood forecasting of Mekerra watershed, Algeria. Arabian Journal of Geosciences, 9(20), 751.

Lievens H, Tomer S.K, Al Bitar A, De Lannoy G. J, Drusch M, Dumedah G, Fransen H.J, Kerr Y.H, Martens B, Pan M. Roundy J. K. (2015). SMOS soil moisture assimilation for improved hydrologic simulation in the Murray Darling Basin Australia. Remote Sens. Environ, 168 146-162

Massari C, Brocca L, Barbetta S, Papathanasiou C, Mimikou M, Moramarco T. (2014). Using globally available soil moisture indicators for flood modelling in Mediterranean catchments. Hydrol. Earth Syst. Sci 18(2) 839-853.

Massari C, Brocca L, Tarpanelli A, Moramarco T. (2015). Data assimilation of satellite soil moisture into rainfall-runoff modelling: A complex recipe?.Remote Sens, 7(9) 11403-11433.

Moriasi DN, Arnold JG, Van Liew MW, Bingner RL, Harmel RD, Veith TL. (2007). Model evaluation guidelines for systematic quantification of accuracy in watershed simulations. Trans. ASABE 50(3) 885-900.

Moulin L., Gaume E., Obled C. (2009). Uncertainties on mean areal precipitation: Assessment and impact on streamflow simulations. Hydrology and Earth System Sciences Discussions, 13(2), 99–114.

Mure-Ravaud M, Binet G, Bracq M, Perarnaud JJ, Fradin A, Litrico X. (2016). A web based tool for operational real-time flood forecasting using data assimilation to update hydraulic states. Environ. Modell. Softw. 84 35-49.

Nester T, Komma J, Blöschl G (2016). Real time flood forecasting in the Upper Danube basin. J Hydrol. Hydromech. 64(4) 404-414.

Neto JG, Ribeiro-Neto A, Montenegro SM. (2014). Assessment of rainfall-runoff models for flood river extreme event simulations. Proceedings of the 6th international conference on flood management pp. 1-10. Sau Paulo Brazil.

Nguyen P, Thorstensen A, Sorooshian S, Hsu K, AghaKouchak A, Sanders B, Koren V, Cui Z. Smith M. (2016). A high resolution coupled hydrologic–hydraulic model (HiResFlood-UCI) for flash flood modeling. J. Hydrol, 541 401-420.

Noh S. J, Lee J. H, Lee S, Kawaike K, Seo D. J. (2018). Hyper-resolution 1D-2D urban flood modelling using LiDAR data and hybrid parallelization. Environ. Modell. Softw, 103 131-145.

Oleyiblo JO, Li ZJ. (2010). Application of HEC-HMS for flood forecasting in Misai and Wan'an catchments in China. Water Sci.Eng, 3(1) 14-22.

Rosburg TT, Nelson PA, Bledsoe BP (2017). Effects of urbanization on flow duration and stream flashiness: a case study of Puget Sound streams, western Washington, USA. JAWRA J. Amer. Water Resour. Assoc. 53(2), 493-507.

Sanders B. F, Schubert J. E. (2019). PRIMo: Parallel raster inundation model. Adv Water Resour, 126 79-95.

Sanz Ramos M, Amengual A, BladéiCastellet E, Romero R, Roux H. (2018). Flood forecasting using a coupled hydrological and hydraulic model (based on FVM) and

highresolution meteorological model. Proceedings of River Flow 2018-Ninth International Conference on Fluvial Hydraulics (pp. 1-8) Lyon France.

Scharffenberg W.A, Fleming M.J. (2006). Hydrologic modeling system HEC- HMS: User's manual. US Army Corps of Engineers Hydrologic Engineering Center.

Schelfaut K, Pannemans B, Van der Craats I, Krywkow J. Mysiak J, Cools J (2011). Bringing flood resilience into practice: the FREEMAN project. Environ. Sci. Pol, 14(7), 825-833.

Schiemann R, Erdin R, Willi M, Frei C, Berenguer M, Sempere-Torres D. (2011). Geostatistical radar-raingauge combination with nonparametric correlograms: methodological considerations and application in Switzerland. Hydrol. Earth Sys. Sci, 15(5) 1515-1536.

Schwanenberg D, Natschke M, Todini E, Reggiani P. (2018). Scientific technical and institutional challenges towards next-generation operational flood risk management decision support systems. Int. J. River Basin Manage 16(3) 345-352.

Shchepetkin AF, McWilliams JC. (2005). The regional oceanic modeling system (ROMS): a split-explicit free-surface topography-following-coordinate oceanic model. Ocean Model.l 9(4) 347-404.

Skamarock W. C, Klemp J. B, Dudhia J, Gill D. O, Barker D. M, Wang W. Powers J. G. (2008). A description of the Advanced Research WRF version 3. NCAR Technical note-475+ STR.

Sopelana J, Cea L, Ruano S. (2018). A continuous simulation approach for the estimation of extreme flood inundation in coastal river reaches affected by meso and macro tides. Nat Haz 93(3) 1337-1358.

Svensson C, Jones D.A. (2002). Dependence between extreme sea surge river flow and precipitation in eastern Britain. Int. J. Climatol 22 1149-1168.

Tayfur G, Zucco G, Brocca L, Moramarco T. (2014). Coupling soil moisture and precipitation observations for predicting hourly runoff at small catchment scale. J. Hydrol. 510 363-371.

Thielen J, Bartholmes J, Ramos MH, Roo AD (2009). The European flood alert system–part 1: concept and development. Hydrol. Earth Sys. Sci 13(2) 125-140.

Thiemig V, Bisselink B, Pappenberger F, Thielen J. (2015). A pan-African medium-range ensemble flood forecast system. Hydrol. Earth Syst. Sci 19(8) 3365-3385.

Unduche F, Tolossa H, Senbeta D, Zhu E (2018). Evaluation of four hydrological models for operational flood forecasting in a Canadian Prairie watershed. Hydrol. Sci. J. 63(8) 1133-1149.

Van Steenbergen N, Willems P. (2013). Increasing river flood preparedness by real-time warning based on wetness state conditions. J. Hydrol. 489 227-237.

Villarini G., Mandapaka PV., Krajewski WF., Moore RJ. (2008). Rainfall and sampling

uncertainties: A rain gauge perspective. Journal of Geophysical Research: Atmospheres, 113(D11)

Wallemarq P, Below R. McLean D. UNISDR and CRED report: Economic Losses, Poverty & Disasters (1998–2017). Technical report, 2018.

Wanders N, Karssenberg D, Roo AD, De Jong SM, Bierkens MFP. (2014). The suitability of remotely sensed soil moisture for improving operational flood forecasting. Hydrol. Earth Syst. Sci, 18(6) 2343-2357.

Weerts AH, Winsemius HC, Verkade JS (2011). Estimation of predictive hydrological uncertainty using quantile regression: examples from the National Flood Forecasting System (England and Wales). Hydrol. Earth Sys. Sci 15(1) 255-265.

Wick G. A, Neiman P. J, Ralph F. M, Hamill T. M. (2013). Evaluation of forecasts of the water vapor signature of atmospheric rivers in operational numerical weather prediction models. Weather Forecast, 28(6) 1337-1352.

Xia X, Liang Q, Ming X. (2019). A full-scale fluvial flood modelling framework based on a high-performance integrated hydrodynamic modelling system (HiPIMS). Adv. Water Resour, 132 103392.

Xunta de Galicia (2016). Plan especial de protección civil ante el riesgo de inundaciones en Galicia. Official Journal.

Zhong H Van Overloop PJ Van Gelder PHAJM (2013) A joint probability approach using a 1D hydrodynamic model for estimating high water level frequencies in the Lower Rhine Delta. Nat. Hazards Earth Syst. Sci. 13 1841–1852.